Contaminant-Source Detection in a Water Distribution System Using the Ensemble Kalman Filter

Ilaria Butera[1], J. Jaime Gómez-Hernández[2], and Silvia Nicotra[3]

[1]Department of Environment, Land and Infrastructure Engineering, Politecnico di Torino. Italy.
Email: ilaria.butera@polito.it

[2]Institute for Water and Environmental Engineering. Universitat Politècnica de València. Spain.
Email: jgomez@upv.es

[3]Department of Environment, Land and Infrastructure Engineering, Politecnico di Torino. Italy.
Email: silvia.nicotra@polito.it

ABSTRACT

Early detection of a contamination leach into a water distribution system, followed by the identification of the source and an evaluation of the total amount of contaminant that has been injected into the system is of paramount importance in order to protect water user's health. The ensemble Kalman filter, which has been recently applied in hydrogeology to detect contaminant sources in aquifers, is extended to the identification of a contaminant source and its intensity in a water distribution system. The driving concept is the assimilation of contaminant observations at the nodes of the pipeline network at specified time intervals until enough information has been collected to allow the positioning of the source and the estimation of its intensity. Several scenarios are analyzed considering sources at different nodes, with different delays between the beginning of the pollution and the start of the measurements, with different sampling time intervals, and with different observation ending times. The scenarios are carried out in the bench-marking Anytown network demonstrating the ability of the ensemble Kalman filter for contaminant-source detection in real water distribution systems. The use of the ensemble Kalman filter supposed a major

breakthrough in the inverse modeling of subsurface flow and transport, the successful results of its application to the synthetic Anytown network warrant further exploration of its capabilities in the realm of water distribution systems.

INTRODUCTION

Water distribution systems (WDSs) are a key infrastructure for the preservation of people's health. Intentional or accidental contamination of the systems has to be detected in the shortest possible period to reduce damages, for which Early Warning Systems are desirable. To limit the damages caused by a contamination event, it is important to detect both the source location and the release intensity; the source location will allow repairing the system and preventing further contamination and the release intensity will allow estimating the amount of contaminant injected.

Measurement networks are being deployed in WDSs to detect the presence of pollutants and a large effort has been done to identify strategies for the optimal location of sensors (e.g., Hart and Murray 2010; Ung et al. 2017). In the last fifteen years, an interest in using the observed concentration measurements at some nodes of the WDS to identify the source location and the release history has grown, and a number of methodologies has been developed; a good review paper on the subject was published by Adedoja et al. (2018). The authors of this review identify three types of approaches: probabilistic approaches, simulation approaches and others, like artificial neutral networks (Kim et al. 2008) or hybrid methods (Liu et al. 2012). A few of the works discussed in the review are worth to be singled out: Tryby et al. (2010) propose an optimal sensor placement design for source identification using minimum least-squares optimization; De Sanctis et al. (2010) use a particle backtracking method to identify the nodes of a network that are coherent with the presence/absence of contamination at sensor locations; Liu et al. (2011) propose an adaptive dynamic optimization procedure for contaminant source identification aimed at avoiding the ill-posedness of the problem; Eliades and Polycarpou (2012) use decision trees to identify the network nodes where the contamination took place with as few manual samplings as possible; Shen and McBean (2012) identify potential intrusion nodes using parallel computing, a large database, and data-mining; Wang and Harrison (2013) implement Markov chain Monte

Carlo for contaminant source identification, although they recognize that further improvements are needed to make the approach operational; Perelman and Ostfeld (2013) use Bayesian networks to estimate the likelihood of the injection location of a contaminant and its propagation into the system; Butera et al. (2013a) use a geostatistical approach to recover the release history of a pollutant intrusion; Yang and Boccelli (2014) mix a Bayesian approach with backtracking to calculate the probabilities of potential source locations; Wang and Harrison (2014) mix a Bayesian approach with support vector machines to improve the likelihood calculations; Seth et al. (2016) propose a systematic procedure for testing and evaluating source identification methods; and Ung et al. (2017) couple an adjoint source identification method and a Monte Carlo sensor placement algorithm to optimally and accurately place sensors. The broad review by Adedoja et al. (2018) highlights the current relevance of the research topic and concludes that more effort is necessary to make these models applicable in real life. It is also worth pointing out that source identification can help in solving the important problem of pathogen intrusion during transients through leaks (Karim et al. 2003; CollIns et al. 2012).

From a mathematical point of view, identifying a contaminant source from some concentration data can be cast as an inverse problem: information about the state of the system is used to identify parameters, boundary conditions or forcing terms of the system, which is modeled by a system state equation. Inverse problems have been addressed for many years in hydrology and hydraulics with both deterministic and stochastic approaches. A good review of inverse models in subsurface hydrology can be found in Zhou et al. (2014), and some applications in surface hydrology in D'Oria et al. (2014), D'Oria et al. (2017) or Todaro et al. (2019). Probably, subsurface hydrology has been the area with the largest body of research in the subject, from the early deterministic works (i.e., de Marsily et al. 1984; Carrera and Neuman 1986) to the later stochastic ones (i.e, Woodbury and Ulrych 1993; Wen et al. 1999; Li et al. 2012; Capilla et al. 1999; Sun et al. 2009; Zhou et al. 2012). In the last decades, the use of the ensemble Kalman filter has gained much attention as an inverse modeling method, even though in its inception it was not considered an inverse model but a filtering algorithm to filter out model and observation error from model pre-

dictions. Applications in hydrogeology (i.e., Franssen and Kinzelbach 2009; Schöniger et al. 2012; Zhou et al. 2012; Xu et al. 2013) and in petroleum engineering (ie.,Wen et al. 1999; Chen et al. 2010) are abundant. Implementations of inverse modeling for the identification of contaminant sources in groundwater can be found in the reviews by Atmadja and Bagtzoglou (2001), Bagtzoglou and Atmadja (2005), Michalak and Kitanidis (2004) or Sun et al. (2006). More recent approaches have used methods based on minimum relative entropy, the geostatistical approach or the use of adjoint states (Bagtzoglou et al. 1992; Butera et al. 2013b; Koch and Nowak 2016; Neupauer and Wilson 1999; Woodbury and Ulrych 1996).

Aquifers and WDS are conceptually similar, in both cases water (and solutes) move in a heterogeneous media, driven mainly by gravity and pumping that induce changes in water pressures and solute concentrations in space and time. In both systems, there is a state equation that permits the prediction of the system state at time t, given the state at time $t - \Delta t$; a state equation that depends on geometrical and material parameters, such as aquifer extension and hydraulic conductivities (in aquifers), or pipe lengths and roughness coefficients (in WDS). These similarities have encouraged some researchers to use approaches that have worked in hydrogeology in WDS. For example, the work by (Butera et al. 2013a) demonstrates the application of the geostatistical approach for the identification of the release history of a contamination event in a WDS. The main difference is that the aquifer state is defined continuously in two-dimensional or three-dimensional space, but WDS state is defined continuously in a number of one-dimensional segments. This difference will require a special treatment as explained later. The motivation of this paper is to demonstrate the application of the ensemble Kalman filter, a technique that recently has demonstrated its potential in groundwater modeling for the purpose of contaminant-source identification (Chen et al. 2018; Xu and Gómez-Hernández 2016; Xu and Gómez-Hernández 2018) to the field of WDS. The ensemble Kalman filter has already been used in WDSs, for instance, (Rajakumar et al. 2019) applied it to model the uncertainty on chlorine concentration or (Ye and Fenner 2014) used it to detect bursts in WDSs, but, to the best of our knowledge, it has not been applied to the problem of contaminant source and release identification. This paper does benchmark the ensemble Kalman

filter against other approaches developed for the same purpose; it shows the potential of a new approach for source identification that is general, simple to understand and implement, and that has proven its effectiveness in other fields. The remainder of this manuscript is organized as follows: a brief description of the ensemble Kalman filter is presented, followed by a description of the case study and finalizing with a discussion of the results and some conclusions.

THE ENSEMBLE KALMAN FILTER

The ensemble Kalman filter (EnKF) was developed by Evensen (1994, 2003) to overcome the difficulties of the Kalman filter to deal with systems that evolve non-linearly in space-time. Although the filter was originally designed to improve the estimation of the state of the system, it has been extended for the estimation of the parameters controlling the state equation, by considering these parameters as state variables as part of what is called an augmented state. The resulting filter with augmented state is a powerful inverse modeling algorithm. The main idea of the filtering algorithm is the sequential forecasting and updating of the augmented state vector, in which the forecasting is based on the state equation, and the updating is based on the discrepancy between observations and predictions to modify the augmented state. This forecast and update steps are repeated each time that a new sets of observations is available. The forecast can be done with regard to the last update of the state variables and using the last update of the system parameters, or it can be done with the state variables from time zero and the last update of the system parameters, in cases in which the update of the state may results in a state spatial distribution that may violate some fundamental laws, such as mass conservation, or, as it will be in this case, the updated parameters modify the way the system would have behaved since time zero. Indeed, in the problem of contaminant source identification, updating the position of the source can only be accounted for to predict the state in the next time step by rerunning the forecast from time zero, when the source enters the system. For this reason, this approach is referred to as the restart ensemble Kalman filter (rEnKF). In this paper, the state variables are solute concentrations and the model parameters to be inverted are the node at which the solute enters the WDS and the release intensity. Let $\mathbf{X}$ be the vector of parameters, and $\mathbf{Y}$ the vector of solute concentrations in the system. They both are related through a state equation

with given boundary, initial conditions and forcing terms,

$$\mathbf{Y}(t) = \psi(\mathbf{X}, \mathbf{Y}(t - \Delta t)), \tag{1}$$

where t indicates time. In general, the state at time t is computed as a function of the state in the previous time step $t - \Delta t$. In the rEnKF with augmented state, the state equation is rewritten as

$$\begin{pmatrix} \mathbf{X}(t) \\ \mathbf{Y}(t) \end{pmatrix} = \begin{pmatrix} \mathbf{X}(t - \Delta t) \\ \psi(\mathbf{X}(t - \Delta t), \mathbf{Y}(0)) \end{pmatrix}. \tag{2}$$

The first step in the rEnKF is the forecast of the (augmented) system state for the next time step. This forecast is performed using the state equation (2), on one hand we forecast the parameters, which remain the same since we have no state equation for its evolution in time, on the other hand we also forecast the state from time zero, this forecast will use the last update of the parameter values, which will be performed in the assimilation step. At time zero, we assume that the contaminant has not entered the system yet and therefore all values of $\mathbf{Y}(0)$ are equal to zero. The second step is the updating of the augmented state once new observations are available. In this specific implementation in which the forecast is always made from the state values at time zero, the interest is in the update of the parameter values, since the updated states will be of no use for the next forecast step. Given a set of state observations $\mathbf{Y}^{obs}(t)$, the discrepancy between forecast values and observed ones will be used to update the parameter forecast in (2)

$$\mathbf{X}^a(t) = \mathbf{X}(t) + \mathbf{G}(t) \left(\mathbf{Y}^{obs}(t) + \mathbf{e}(t) - \mathbf{Y}(t) \right), \tag{3}$$

where $\mathbf{X}^a(t)$ is the updated parameters values after data assimilation, $\mathbf{e}(t)$ is the observation error with zero mean and covariance given by the matrix $\mathbf{R}(t)$, and $\mathbf{G}(t)$ is the Kalman gain, given by

$$\mathbf{G}(t) = \mathbf{C}_{XY}(t) \left(\mathbf{C}_{YY}(t) + \mathbf{R}(t) \right)^{-1}, \tag{4}$$

where $\mathbf{C}_{XY}(t)$ is the covariance between all the parameters and the state variables at observation locations, and $\mathbf{C}_{YY}(t)$ is the covariance of the state variable at observation locations. Therefore, if there are n_p parameters and n_o observations locations, vectors $\mathbf{X}^a(t)$ and $\mathbf{X}(t)$ have sizes $n_p \times 1$, vectors $\mathbf{Y}^{obs}(t)$, $\mathbf{e}(t)$ and $\mathbf{Y}(t)$ have sizes $n_o \times 1$, the Kalman gain $\mathbf{G}(t)$ is a matrix of size $n_p \times n_o$, the covariance $\mathbf{C}_{XY}$ is a matrix of size $n_p \times n_o$, and the matrices $\mathbf{C}_{YY}(t)$ and $\mathbf{R}(t)$ are of size $n_o \times n_o$, with the matrix $\mathbf{R}(t)$ generally being a diagonal matrix when the observation errors are modeled as uncorrelated. The Kalman gain is a unique matrix that is computed after each observation step and used to update all realizations.

In the earlier versions of the Kalman filter and the extended Kalman filter, the covariance matrices were computed using the state equation. Such a computation is exact if the state equation is linear, but it is only approximate if it is not linear. The ensemble Kalman filter solves the problem of computing the covariances for non-linear state transition equations. In the EnKF formulation, the covariances in Eq. (4) are estimated from an ensemble of realizations of parameters and state variables (calculated according to the state equation) in which each realization goes through the two steps of forecast and update described above. It is after the forecast step that the covariances matrices are calculated; specifically, the two covariances involved in the computation of the Kalman gain are estimated from a set of N ensemble realizations as

$$\mathbf{C}_{XY}(t) = \frac{1}{N-1}\left((\overline{\overline{\mathbf{X}}} - \overline{\mathbf{X}}\mathbf{1}_{1\times N})(\overline{\overline{\mathbf{Y}}} - \overline{\mathbf{Y}}\mathbf{1}_{1\times N})^T\right), \tag{5}$$

$$\mathbf{C}_{YY}(t) = \frac{1}{N-1}\left((\overline{\overline{\mathbf{Y}}} - \overline{\mathbf{Y}}\mathbf{1}_{1\times N})(\overline{\overline{\mathbf{Y}}} - \overline{\mathbf{Y}}\mathbf{1}_{1\times N})^T\right), \tag{6}$$

where $\mathbf{1}_{1\times N}$ represents a row vector with N ones, $\overline{\overline{\mathbf{X}}}$ is a matrix of size $n_p \times N$ in which each column contains the parameters values of a realization, $\overline{\mathbf{X}}$ is a column vector of size $n_p \times 1$ with the average values of each parameter computed through the realizations $\overline{\mathbf{X}} = \frac{1}{N}\overline{\overline{\mathbf{X}}}\mathbf{1}_{N\times 1}$ (now $\mathbf{1}_{N\times 1}$ is a column vector with N ones) , and, similarly, $\overline{\overline{\mathbf{Y}}}$ is a matrix of size $n_o \times N$ in which each column contains the forecast concentrations at observation locations, and $\overline{\overline{\mathbf{Y}}}$ is a column vector of size $n_o \times 1$ with the average state values at each observation location computed through the ensemble of realizations

$\overline{\mathbf{Y}} = \frac{1}{N}(\overline{\overline{\mathbf{Y}}}\mathbf{1}_{N\times 1})$.

The restart ensemble Kalman filter workflow is as follows:

1. Set the initial state of the system $\overline{\overline{\mathbf{Y}}}(0)$, and generate an initial ensemble of N realizations of the parameters to be identified $\overline{\overline{\mathbf{X}}}(0)$ then, repeat the following steps for as many time steps as observations are available.
2. For each realization, forecast the state of the system to the next time step for which observations are available using Eq. (2). In this case, a solute transport model is used for the forecast.
3. Extract the forecast values at observed locations from all realizations, build matrices $\overline{\overline{\mathbf{X}}}$ and $\overline{\overline{\mathbf{Y}}}$, and compute the covariances in Eqs. (5) and (6)
4. Compute the Kalman gain in Eq. (4).
5. For each realization, update the parameter values using Eq. (3).
6. Go back to 2 while new observations are sampled.

The ensemble of realizations provides a set of values for each parameter, which will converge to a final set of ensemble values the mean of which should be close to the actual parameter value and the variance of which gives an estimate of the uncertainty about the estimation. At time zero, the mean and variance of the parameters are those of the random functions used to generate them at step 1 of the workflow; then, the ensembles of updated parameters should narrow their variability and converge towards the underlying values. The main problem of the ensemble Kalman filter occurs when the ensemble of realizations collapses onto a single value which is far from the actual value (i.e., Xu et al. 2013). This is referred to as filter collapsing, or filter inbreeding and it is generally related to an underestimation of the covariance in Eqs. (6) and (5).

In the present application, the algorithm will be used for the identification of three parameters, the two spatial coordinates of the source and the logarithm of the release intensity of the contamination injected into the system. The use of the logarithm of the intensity is because the updating equation (3) does not preclude the updated values to be negative, while working with logarithms,

positive release intensities will be ensured.

CASE STUDY

This is an academic exercise in the absence of real data. It is intended to solve a set of different scenarios, each with a predefined source location and intensity. To expand the casuistry, up to 16 different scenarios will be considered, with the source located in each case at a different node in the network, and for all of them a mass flux intensity of 100 mg·min^{-1} will be assumed. Such an intensity results in concentrations in the network in the order of hundredths of mg·l^{-1}. As in this case the location of the source is known in advance for each scenario, the goal is that the evolution of the $\mathbf{X}^a(t)$, as new measurements are assimilated at each step, leads to the predefined location and intensity of the source considered for each scenario. In a real case, such location and intensity will not be known in advance, in such a case, the prediction will be given by the average of the ensemble of realizations and the prediction uncertainty by their standard deviation.

The application of the rEnKF for the identification of the location and intensity of a contaminant release into a WDS is applied to the Anytown network of Walski et al. (1987), a common benchmark in water supply analysis. The Anytown network is composed of 16 nodes (not sequentially numbered) and 32 links of lengths varying between 1828.8 m and 3657.7 m, which is sketched in Fig. 1a. Water is supplied from groundwater resources through a pumping system into two storage tanks. The daily mean discharge supplied by the network is equal to 365 l·s^{-1}. Hourly patterns are used to simulate a time variable demand, with values that go from 325 l·s^{-1} to 475 l·s^{-1}. Pipeline roughness is described using a Hazen-Williams C-factor, which varies between 70 and 120.

A contaminant release of uniform intensity occurs in one of the 16 nodes of the system. The release intensity, i, and the spatial coordinates of the source (x, y) are the three parameters to identify by the rEnKF. The contaminant is a non-reactive solute; however, the proposed methodology could be applied to reactive solutes simply modifying the state equation to account for the reactions. The contaminant enters the system as a single source; the problem of multiple sources or varying intensity sources has not been considered in this manuscript but deserves further consideration. The software used to simulate the flow and transport in the pipe network is version 2.2 of EPANET

Rossman 2000.

The simulation of the contaminant evolution in the perfectly known Anytown system is sampled at all nodes at specified times. These samples will be the observations against which the forecasted values during the application of the EnKF will be contrasted.

The contaminant sensors, located in all 16 nodes of the network, are activated at certain time t_1 after the release happens and measure the concentration at time increments Δt. They stop measuring after a certain t_{max}. In the following, a number of scenarios will be run to try to analyze the impact of t_1. The meaning of t_1 is associated to the idea that the sensors may not be continuously running at all times, and that they only start measuring after some warning (collected by other means than the sensors) is received and then an operator activates them. This activation could be immediate (if the sensors are continuously monitoring) or it can be later (if the sensors are activately manually after a warning), once the contaminant has already spread through the pipeline system. The scenarios will analyze also the impact of the sampling interval size, Δt; and the impact of the magnitude of t_{max}, the time at which the system stops measuring, a small value of it will replicate a possible rupture of the sensor system.

The rEnKF starts with an ensemble of realizations for the three parameters. The number of realizations was initially 100 but it was reduced down to 48 when it was found that similar results were found with this smaller number. The initial set of coordinates for the 48 realizations is fixed and the same for all scenarios and realizations. It is shown in Fig. 1c. Notice that the source initial locations coincide with all nodes of the system plus the center point of all pipes. The initial set of release intensities is distributed uniformly in $[0.5I_1, 2I_1]$, where I_1 is the release intensity estimated at time t_1 when the sensors perform the first observation of concentrations and fluxes at all 16 nodes and given by:

$$I_1 = \sum_{i=1}^{16} C_i(t_1) Q_i(t_1). \tag{7}$$

Measurement errors are modeled with a zero mean and a diagonal covariance matrix, $\mathbf{R} = \sigma_e^2 \mathcal{I}$, with $\sigma_e^2 = 10^{-5}$ mg^{2}l^{-2}, with $\mathcal{I}$ being the identity matrix. This small measurement error variance

is coherent with the concentrations observed in the network, which vary between 0 and 0.05 $mg \cdot l^{-1}$. (These concentrations are consistent with an injection of 100 $mg \cdot min^{-1}$.)

During the forecast step, if the concentrations modeled were below 10^{-6} $mg \cdot l^{-1}$, the concentration was set to zero to mimic the detection limit of the sensors.

During the forecast step, model uncertainties are introduced by adding an error to the base demand at each node from a distribution of zero mean and standard deviation equal to 5% of the base demand value.

During the updating step of the rEnKF, the coordinates of the source will be updated to some values in the XY plane that will not necessarily fall on the pipeline system; for this reason, the updated coordinate values resulting from the application of Eq. (3) to all the realizations are relocated to the closest node on the discretized pipeline system shown in Fig. 1b.

During the updating step and in order to prevent filter collapsing, it is convenient to inflate the covariance matrix, C_{YY}. After some tests, it was found that multiplying the diagonal of C_{YY} by 1.1 gives stable results.

RESULTS AND DISCUSSION

As already mentioned, a preliminary analysis was performed to decide on the size of the ensemble and it was found that an ensemble of 48 realizations gave as good results as an ensemble of 100 realizations, so it was decided to perform all analyses with $N = 48$.

In total, 16 scenarios have been considered with varying source locations, sensor start time after release, maximum monitoring time, and interval between measurements. The combinations of these values for each scenario are shown in Table 1.

In order to quantify the performance of the rEnKF in each scenario, four indicators are built. The first one measures the lack of precision or the spread of the ensemble of coordinate realizations at the end of the assimilation process by computing the square root of the moment of inertia of these coordinates with respect to their center of mass. The second one measures the bias or the lack of accuracy of the final ensemble of coordinate realizations by computing the square root of the moment of inertia of these coordinates with respect to the true source location. In both cases,

these values are normalized by the corresponding values computed with the coordinate realizations at time zero. Similarly, to evaluate the uncertainty of the release intensities at the end of the assimilation process, its coefficient of variation is computed, and to evaluate their bias the square root of the average square deviation between the ensemble intensities and the true one is computed and normalized by the true release intensity. These indicators have the following expressions

$$i_1(t) = \sqrt{\frac{\sum_{j=1}^{N} d_j^2(t)}{\sum_{j=1}^{N} d_j^2(0)}}, \tag{8}$$

$$i_2(t) = \sqrt{\frac{\sum_{j=1}^{N} s_j^2(t)}{\sum_{j=1}^{N} s_j^2(0)}}, \tag{9}$$

$$i_3(t) = \frac{\sigma_I}{\overline{I}}, \tag{10}$$

$$i_4(t) = \frac{\sqrt{\frac{1}{N}\sum_{j=1}^{N}(I_j - I_s)^2}}{I_s}, \tag{11}$$

where N is the number of realizations of the ensemble, $\{d_j, j = 1, \ldots, N\}$ are the distances between each realization position and their center of mass, $\{s_j, j = 1, \ldots, N\}$ are the distances between the each realization position and the true release location, $\{I_j, j = 1, \ldots, N\}$ are the ensemble intensities, σ_I is the standard deviation of this ensemble, $\overline{I}$ is the mean of this ensemble, and I_S is the true release intensity. Notice that these indicators are computed at the end of each assimilation step and their evolution in time measure the speed of convergence of the algorithm.

These indicators can be calculated in this case since this is an academic exercise. In a real situation, only indicators i_1 and i_3 could be computed and the success of the approach would be measured by the effective identification of the source.

The values of the four indicators together with the average distance between the ensemble of coordinate realizations and the true source location and the average difference between the ensemble of source intensities and the true one are shown in Table 2.

First thing to notice is that, for scenarios S1 and S7 the identification of the source coordinates is perfect, in both cases the sensor sampling starts late and the sampling interval is short. Fig 2

shows a histogram of i_1 and i_2 computed at the end of the sampling for all scenarios, recall that they measure, respectively, the intrinsic spread of the ensemble of source positions and the bias with respect to the true value relative to the spread and bias of the initial source locations of Fig 1c. For all cases, the spread measured by i_1 is reduced drastically to below 4% of the initial value, but the bias measured by i_2 is kept at relatively larger values for a number of scenarios. The large bias in scenario 8 (source at node 11) may be explained by the late start of the sensors, the biases for scenarios 15 (source at 18) and 16 (source at 19) may be explained by the complex flow patterns through these nodes linking several pipes. However, overall, the estimation of the source locations is good to very good for all cases since the average deviation of the final positions from the true locations are, for all cases, below 150 m, a small value compared with the pipe lengths, which range between 1828 m and 3568 m.

Fig. 3 shows a histogram of i_3 and i_4 computed at the end of the sampling for all scenarios. The spreads and the biases are always reduced below 10% of their initial values and for some scenarios below 2%. The average difference between the final ensemble of intensities and the true value is always small, less than ± 7 mg·min^{-1}, except for S13. These results are indicative of a very good identification of the release intensity. The worst estimates occur for scenarios 5, 6, 12, 13 and 16. Scenarios 5 and 6 could be explained by a late start of the sampling process and the location of the sources along the edge of the network (sources at nodes 8 and 9, respectively) but the behavior of 12, 13 and 16 is more difficult to explain (although it is worth to point out that, for these cases, the source nodes, 15, 16 and 19, are linked by three pipes in the center of the network).

Fig. 4 shows the time evolution of i_1 and i_2 for case 6 (source at node 9) with a late start of the sampling and a long sampling interval; this figure also shows the positions of the source location realizations at $t_{max} = 600$ min. It is interesting to see how, after a few samples, both i_1 and i_2 are down to their minimum values, and how the final source location realizations are all very close to or at the true source locations. Similar results are shown in Fig. 5 for scenario 12 with a release from node 15. This scenario was not one of the best performers in terms of the indicators, yet, even if the final set of realizations is biased with respect to the true source, the final estimate is close to

the true source.

Fig. 6 shows the time evolution of i_3 and i_4 for scenarios 6 and 12 that differ in the starting time of the sampling. The most noticeable item is the large spread and bias of the updated intensities during the first time steps and the sharp decrease of them as more concentrations are assimilated. It also shows that starting the sampling as early as possible can help in identifying the release intensity quickly.

In general, it can be concluded that an early detection of the release (i.e., activating the sensors 60 minutes after the release) followed by a continued sampling at a low frequency (i.e., every 30 minutes) is preferable than a late detection (i.e., activating the sensors 180 minutes after the release) followed by a high-frequency sampling (i.e., every 10 minutes).

Finally, to illustrate the updating process of the source locations, the time evolution of the ensemble of locations for scenarios 7 and 10 (release nodes 10 and 13, respectively) is shown in Figs. 7 and 8, respectively. It is interesting to see how the source locations are being updated after each observation to positions closer and closer to the true source until all ensemble converges onto it.

The AnyTown network may be considered a simple network compared to a real network that could have up to 10,000 nodes for 100,000 inhabitants. The simple case was chosen to test a new approach that had never been tested in water distribution systems. Given its satisfactory results, and considering that in hydrogeology, the EnKF has been applied to numerical models with tens of thousands of discretizing elements, the method should also work in larger systems, with larger computational times.

CONCLUSIONS

This work proposes an application of the restart ensemble Kalman filter (rEnKF) to the identification of the source location and intensity of a contaminant release in a water distribution system. The method proposed has been tested in the Anytown network assuming a constant contaminant injection. Contaminant observations at the nodes of the network are made with varying sampling intervals and sampling start times since the release began. The exercise also considered a small

sampling error and errors in the estimation of the demand at each node. Sixteen scenarios were analyzed in order to reproduce different measurement schemes. From the analysis it is concluded that is best to detect the contamination as soon as possible, followed by a not necessarily very high measurement frequency, for, after a few sampling steps, identify the source location and the release intensity of the contamination release. Despite the small number of ensemble members (only 48) the method proved to successfully identify the source location and release intensity. It is concluded that the rEnKF is a valuable technique for source identification in water distribution systems. Future research should include more realistic cases, with smaller number of sensors, releases occurring anywhere in the network, non uniform releases, and larger sampling errors and modeling errors.

DATA AVAILABILITY

All data, models, or code that support the findings of this study are available from the corresponding author upon reasonable request.

REFERENCES

Adedoja, O. S., Hamam, Y., Khalaf, B., and Sadiku, R. (2018). "Towards development of an optimization model to identify contamination source in a water distribution network." *Water*, 10(5), 579.

Atmadja, J. and Bagtzoglou, A. C. (2001). "State of the Art Report on Mathematical Methods for Groundwater Pollution Source Identification." *Environmental Forensics*, 2(3), 205–214.

Bagtzoglou, A. C. and Atmadja, J. (2005). "Mathematical Methods for Hydrologic Inversion: The Case of Pollution Source Identification." *Water Pollution*, 5, 65–96.

Bagtzoglou, A. C., Dougherty, D. E., and Tompson, A. F. B. (1992). "Application of particle methods to reliable identification of groundwater pollution sources." *Water Resources Management*, 6(1), 15–23.

Butera, I., Boano, F., Revelli, R., and Ridolfi, L. (2013a). "Recovering the release history of a pollutant intrusion into a water supply system through a geostatistical approach." *Journal of Water Resources Planning and Management*, 139(4), 418–425.

Butera, I., Tanda, M. G., and Zanini, A. (2013b). "Simultaneous identification of the pollutant release history and the source location in groundwater by means of a geostatistical approach." *Stochastic Environmental Research and Risk Assessment*, 27(5), 1269–1280.

Capilla, J. E., Rodrigo, J., and Gómez-Hernández, J. J. (1999). "Simulation of non-gaussian transmissivity fields honoring piezometric data and integrating soft and secondary information." *Mathematical Geology*, 31(7), 907–927.

Carrera, J. and Neuman, S. P. (1986). "Estimation of aquifer parameters under transient and steady state conditions: 1. maximum likelihood method incorporating prior information." *Water Resources Research*, 22(2), 199–210.

Chen, Y., Oliver, D. S., et al. (2010). "Parameterization techniques to improve mass conservation and data assimilation for ensemble kalman filter." *SPE Western Regional Meeting*, Society of Petroleum Engineers.

Chen, Z., Gómez-Hernández, J. J., Xu, T., and Zanini, A. (2018). "Joint identification of contaminant source and aquifer geometry in a sandbox experiment with the restart ensemble kalman filter." *Journal of hydrology*, 564, 1074–1084.

CollIns, R. P., BoxAll, J. B., KARneY, B. W., Brunone, B., and Meniconi, S. (2012). "How severe can transients be after a sudden depressurization?." *Journal-American Water Works Association*, 104(4), E243–E251.

de Marsily, G., Lavedan, G., Boucher, M., and FASAMINO, G. (1984). "Interpretation of interference tests in a well field using geostatistical techniques to fit the permeability distribution in a reservoir model." *Geostatistics for natural resources characterization. NATO advanced Study Institute*, 831–849.

De Sanctis, A. E., Shang, F., and Uber, J. G. (2010). "Real-time identification of possible contamination sources using network backtracking methods." *Journal of Water Resources Planning and Management*, 136(4), 444–453.

D'Oria, M., Ferrari, A., Mignosa, P., Tanda, M. G., and Vacondio, R. (2017). "Reverse flow routing in a bayesian framework using a gpu-accelerated 2d shallow water model." *AGUFM*, 2017,

H11E–1218.

D'Oria, M., Mignosa, P., and Tanda, M. G. (2014). "Bayesian estimation of inflow hydrographs in ungauged sites of multiple reach systems." *Advances in water resources*, 63, 143–151.

Eliades, D. G. and Polycarpou, M. M. (2012). "Water contamination impact evaluation and source-area isolation using decision trees." *Journal of Water Resources Planning and Management*, 138(5), 562–570.

Evensen, G. (1994). "Sequential data assimilation with a nonlinear quasi-geostrophic model using Monte Carlo methods to forecast error statistics." *Journal of Geophysical Research*, 99(C5), 10143.

Evensen, G. (2003). "The Ensemble Kalman Filter: Theoretical formulation and practical implementation." *Ocean Dynamics*, 53(4), 343–367.

Franssen, H. H. and Kinzelbach, W. (2009). "Ensemble kalman filtering versus sequential self-calibration for inverse modelling of dynamic groundwater flow systems." *Journal of Hydrology*, 365(3-4), 261–274.

Hart, W. E. and Murray, R. (2010). "Review of sensor placement strategies for contamination warning systems in drinking water distribution systems." *Journal of Water Resources Planning and Management*, 136(6), 611–619.

Karim, M. R., Abbaszadegan, M., and LeChevallier, M. (2003). "Potential for pathogen intrusion during pressure transients." *Journal-American Water Works Association*, 95(5), 134–146.

Kim, M., Choi, C. Y., and Gerba, C. P. (2008). "Source tracking of microbial intrusion in water systems using artificial neural networks." *Water research*, 42(4-5), 1308–1314.

Koch, J. and Nowak, W. (2016). "Identification of contaminant source architectures - A statistical inversion that emulates multiphase physics in a computationally practicable manner." *Water Resources Research*, 52(2), 1009–1025.

Li, L., Zhou, H., Hendricks Franssen, H.-J., and Gómez-Hernández, J. J. (2012). "Modeling transient groundwater flow by coupling ensemble kalman filtering and upscaling." *Water Resources Research*, 48(1).

Liu, L., Ranjithan, S. R., and Mahinthakumar, G. (2011). "Contamination source identification in water distribution systems using an adaptive dynamic optimization procedure." *Journal of Water Resources Planning and Management*, 137(2), 183–192.

Liu, L., Zechman, E. M., Mahinthakumar, G., and Ranji Ranjithan, S. (2012). "Identifying contaminant sources for water distribution systems using a hybrid method." *Civil Engineering and Environmental Systems*, 29(2), 123–136.

Michalak, A. M. and Kitanidis, P. K. (2004). "Estimation of historical groundwater contaminant distribution using the adjoint state method applied to geostatistical inverse modeling." *Water Resources Research*, 40(8).

Neupauer, R. M. and Wilson, J. L. (1999). "Adjoint method for obtaining backward-in-time location and travel time probabilities of a conservative groundwater contaminant." *Water Resources Research*, 35(11), 3389–3398.

Perelman, L. and Ostfeld, A. (2013). "Bayesian networks for source intrusion detection." *Journal of Water Resources Planning and Management*, 139(4), 426–432.

Rajakumar, A. G., Mohan Kumar, M., Amrutur, B., and Kapelan, Z. (2019). "Real-time water quality modeling with ensemble kalman filter for state and parameter estimation in water distribution networks." *Journal of Water Resources Planning and Management*, 145(11), 04019049.

Rossman, L. A. (2000). "Epanet 2: users manual.

Schöniger, A., Nowak, W., and Hendricks Franssen, H.-J. (2012). "Parameter estimation by ensemble kalman filters with transformed data: Approach and application to hydraulic tomography." *Water Resources Research*, 48(4).

Seth, A., Klise, K. A., Siirola, J. D., Haxton, T., and Laird, C. D. (2016). "Testing contamination source identification methods for water distribution networks." *Journal of Water Resources Planning and Management*, 142(4), 04016001.

Shen, H. and McBean, E. (2012). "False negative/positive issues in contaminant source identification for water-distribution systems." *Journal of Water Resources Planning and Management*, 138(3), 230–236.

Sun, A. Y., Morris, A. P., and Mohanty, S. (2009). "Sequential updating of multimodal hydrogeologic parameter fields using localization and clustering techniques." *Water Resources Research*, 45(7).

Sun, A. Y., Painter, S. L., and Wittmeyer, G. W. (2006). "A constrained robust least squares approach for contaminant release history identification." *Water Resources Research*, 42(4), 1–13.

Todaro, V., D'Oria, M., Tanda, M. G., and Gómez-Hernández, J. J. (2019). "Ensemble smoother with multiple data assimilation for reverse flow routing." *Computers & Geosciences*, 131, 32–40.

Tryby, M. E., Propato, M., and Ranjithan, S. R. (2010). "Monitoring design for source identification in water distribution systems." *Journal of Water Resources Planning and Management*, 136(6), 637–646.

Ung, H., Piller, O., Gilbert, D., and Mortazavi, I. (2017). "Accurate and optimal sensor placement for source identification of water distribution networks." *Journal of Water Resources Planning and Management*, 143(8), 04017032.

Walski, T. M., Brill Jr, E. D., Gessler, J., Goulter, I. C., Jeppson, R. M., Lansey, K., Lee, H.-L., Liebman, J. C., Mays, L., Morgan, D. R., et al. (1987). "Battle of the network models: Epilogue." *Journal of Water Resources Planning and Management*, 113(2), 191–203.

Wang, H. and Harrison, K. W. (2013). "Bayesian update method for contaminant source characterization in water distribution systems." *Journal of Water Resources Planning and Management*, 139(1), 13–22.

Wang, H. and Harrison, K. W. (2014). "Improving efficiency of the bayesian approach to water distribution contaminant source characterization with support vector regression." *Journal of Water Resources Planning and Management*, 140(1), 3–11.

Wen, X.-H., Capilla, J. E., Deutsch, C., Gómez-Hernández, J., and Cullick, A. (1999). "A program to create permeability fields that honor single-phase flow rate and pressure data." *Computers & Geosciences*, 25(3), 217–230.

Woodbury, A. D. and Ulrych, T. J. (1993). "Minimum relative entropy: Forward probabilistic modeling." *Water Resources Research*, 29(8), 2847–2860.

494 Woodbury, A. D. and Ulrych, T. J. (1996). "Minimum relative entropy inversion: Theory and
495 application to recovering the release history of a groundwater contaminant." *Water Resources*
496 *Research*, 32(9), 2671–2681.

497 Xu, T. and Gómez-Hernández, J. J. (2016). "Joint identification of contaminant source location,
498 initial release time, and initial solute concentration in an aquifer via ensemble Kalman filtering."
499 *Water Resources Research*.

500 Xu, T. and Gómez-Hernández, J. J. (2018). "Simultaneous identification of a contaminant source
501 and hydraulic conductivity via the restart normal-score ensemble Kalman filter." *Advances in*
502 *Water Resources*, 112(July 2017), 106–123.

503 Xu, T., Gómez-Hernández, J. J., Zhou, H., and Li, L. (2013). "The power of transient piezometric
504 head data in inverse modeling: An application of the localized normal-score enkf with covariance
505 inflation in a heterogenous bimodal hydraulic conductivity field." *Advances in water resources*,
506 54, 100–118.

507 Yang, X. and Boccelli, D. L. (2014). "Bayesian approach for real-time probabilistic contami-
508 nation source identification." *Journal of Water Resources Planning and Management*, 140(8),
509 04014019.

510 Ye, G. and Fenner, R. A. (2014). "Study of burst alarming and data sampling frequency in water dis-
511 tribution networks." *Journal of Water Resources Planning and Management*, 140(6), 06014001.

512 Zhou, H., Gómez-Hernández, J. J., and Li, L. (2014). "Inverse methods in hydrogeology: Evolution
513 and recent trends." *Advances in Water Resources*, 63, 22–37.

514 Zhou, H., Li, L., Franssen, H.-J. H., and Gómez-Hernández, J. J. (2012). "Pattern recognition in
515 a bimodal aquifer using the normal-score ensemble kalman filter." *Mathematical Geosciences*,
516 44(2), 169–185.

List of Tables

TABLE 1. Scenarios considered

Scenario	Source location node number	Source intensity mg·min^{-1}	t_1 min	t_{max} min	Δt min
S1	1	100	180	360	10
S2	2	100	60	300	30
S3	3	100	180	430	10
S4	4	100	60	300	30
S5	8	100	180	600	10
S6	9	100	180	600	30
S7	10	100	180	600	10
S8	11	100	180	600	10
S9	12	100	60	390	30
S10	13	100	60	360	30
S11	14	100	180	600	10
S12	15	100	60	390	30
S13	16	100	180	600	10
S14	17	100	180	600	10
S15	18	100	60	200	10
S16	19	100	60	300	30

TABLE 2. Indicators

Scenario	$i_1(t_{max})$ $\cdot 10^{-2}$	$i_2(t_{max})$ $\cdot 10^{-2}$	$i_3(t_{max})$ $\cdot 10^{-2}$	$i_4(t_{max})$ $\cdot 10^{-2}$	Average distance from source location in m at t_{max}	Average difference from true intensity in mg·min^{-1} at t_{max}
S1	0.00	0.00	0.04	0.43	0.00	-0.43
S2	2.90	1.76	2.94	5.03	16.23	4.02
S3	0.27	1.73	1.82	4.25	18.62	3.82
S4	0.92	1.74	4.84	6.96	16.33	-5.27
S5	0.00	4.15	5.05	7.87	36.38	5.83
S6	4.77	3.39	7.00	9.12	40.95	-6.41
S7	0.00	0.00	0.00	0.13	0.00	3.46
S8	1.83	15.74	5.58	0.32	148.00	-6.34
S9	0.00	8.86	3.38	0.23	69.16	4.73
S10	0.84	0.40	1.67	1.65	2.88	0.10
S11	1.21	0.74	0.96	1.93	5.18	-1.69
S12	1.75	3.14	5.71	6.33	21.41	2.55
S13	0.11	7.23	1.59	12.85	47.35	12.73
S14	0.00	3.04	1.86	1.87	25.18	-0.35
S15	0.00	18.93	2.17	2.90	117.38	-1.99
S16	1.82	20.17	5.72	7.54	118.16	4.67

List of Figures

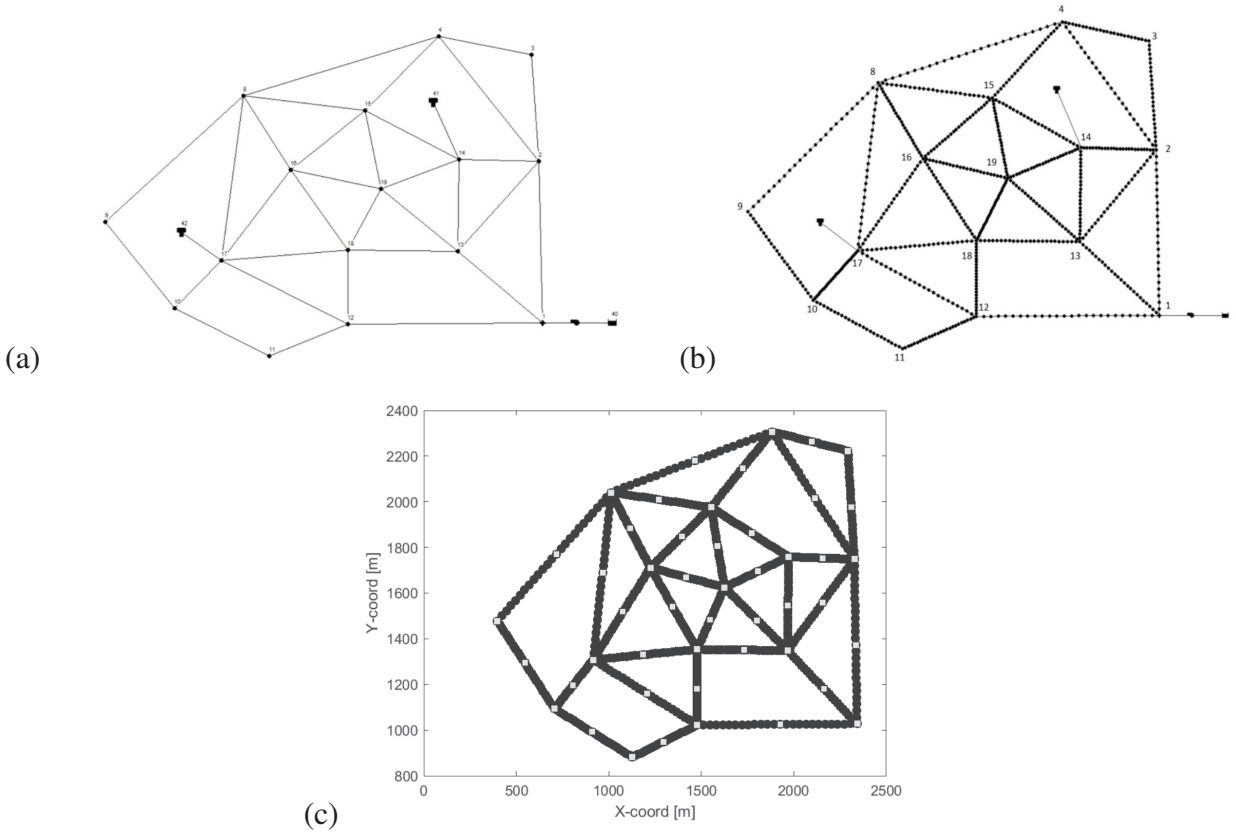

Fig. 1. Sketch of the Anytown WDS, (a) original, (b) with all pipes discretized, and (c) with an indication of the ensemble of 48 initial release locations.

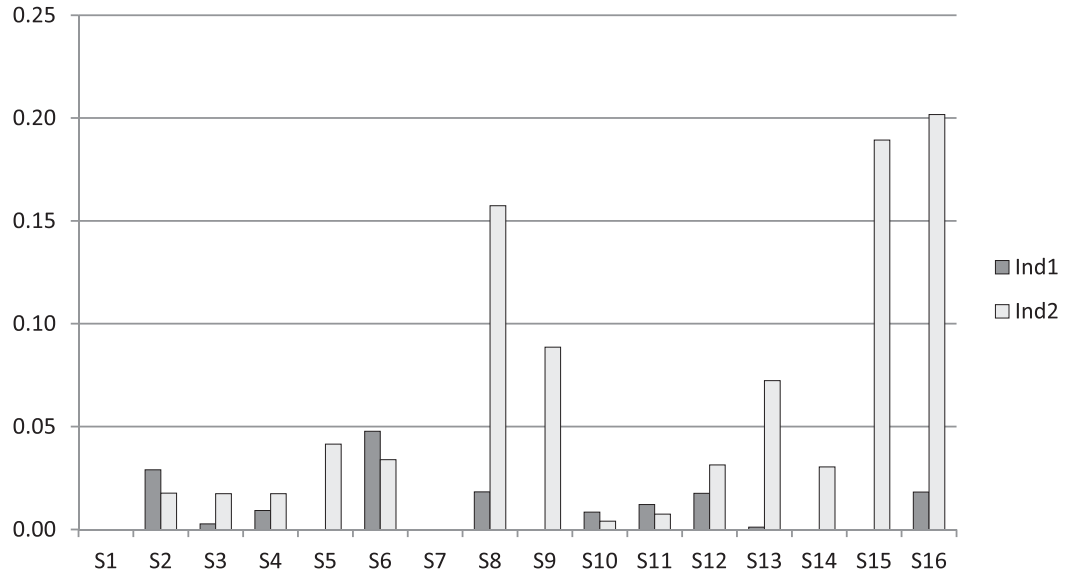

Fig. 2. Histograms of indicators i_1 (coordinate spread) and i_2 (coordinate bias) for all scenarios at $t = t_{max}$.

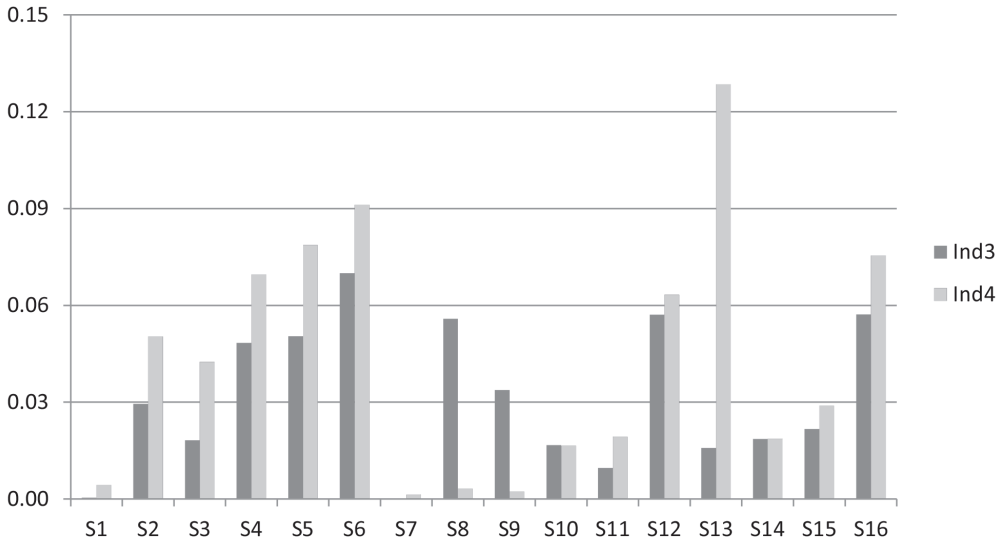

Fig. 3. Histograms of indicators i_3 (intensity spread) and i_4 (intensity bias) for all scenarios at $t = t_{max}$.

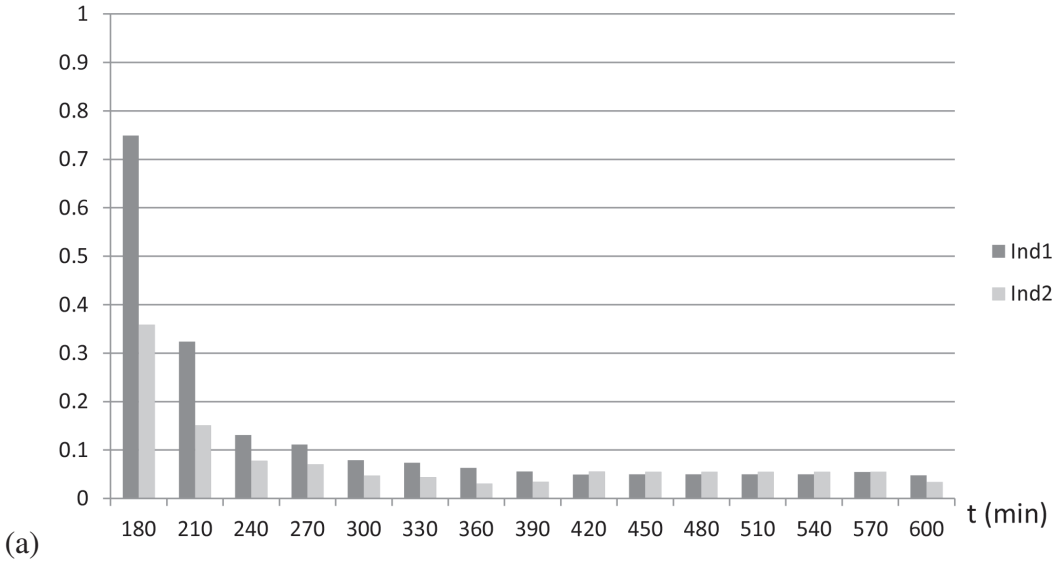

(a)

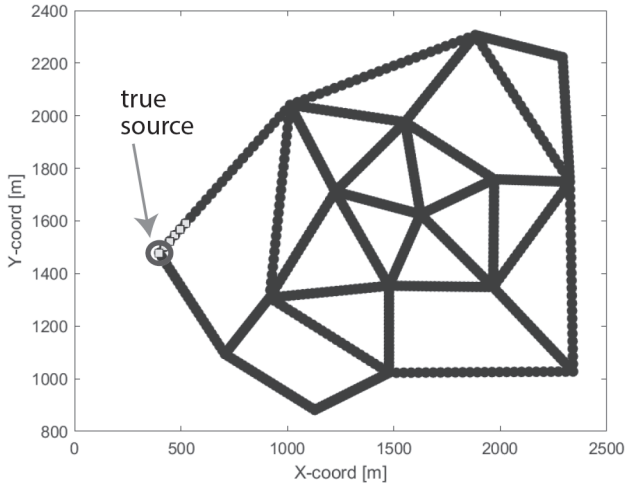

(b)

Fig. 4. Scenario 6. (a) Time evolution of i_1 and i_2. (b) Spatial distribution of the source estimate positions of all 48 realizations at time t_{max} (light squares).

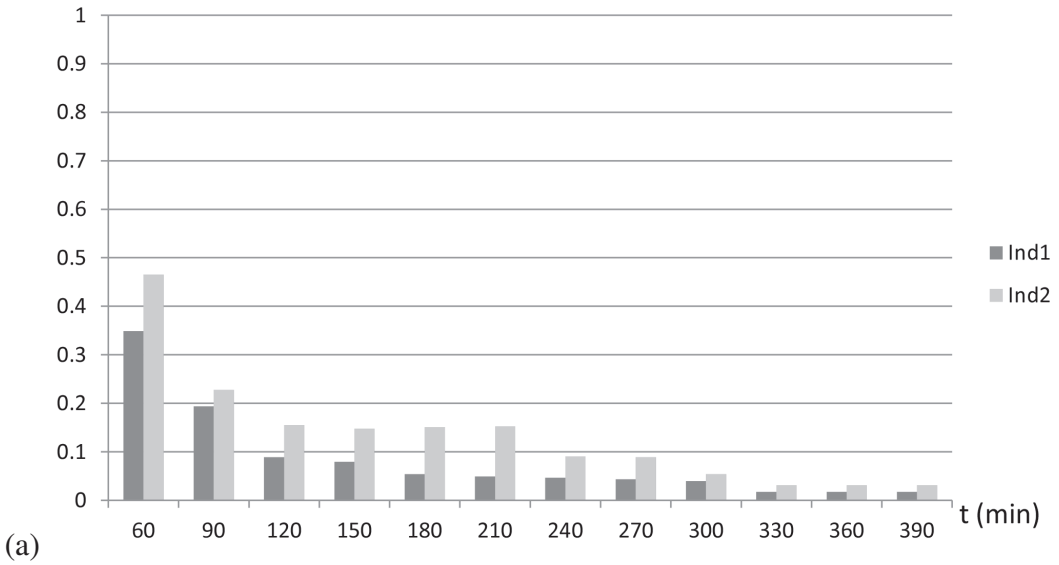

(a)

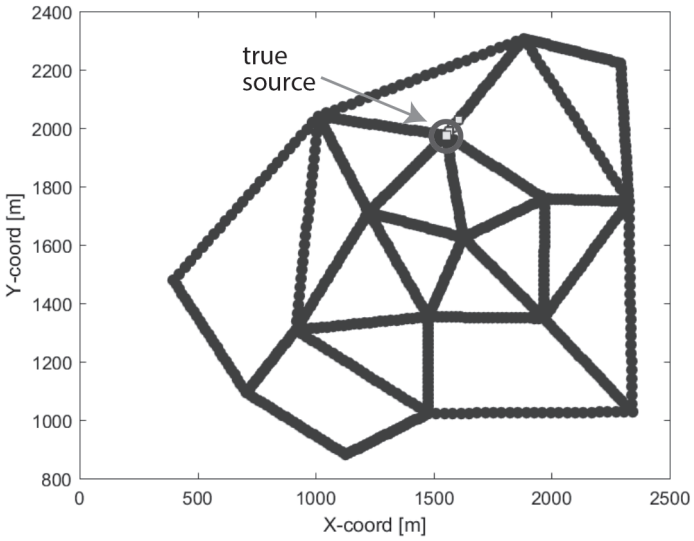

(b)

Fig. 5. Scenario 12. (a) Time evolution of i_1 and i_2. (b) Spatial distribution of the source estimate positions of all 48 realizations at time t_{max} (light squares).

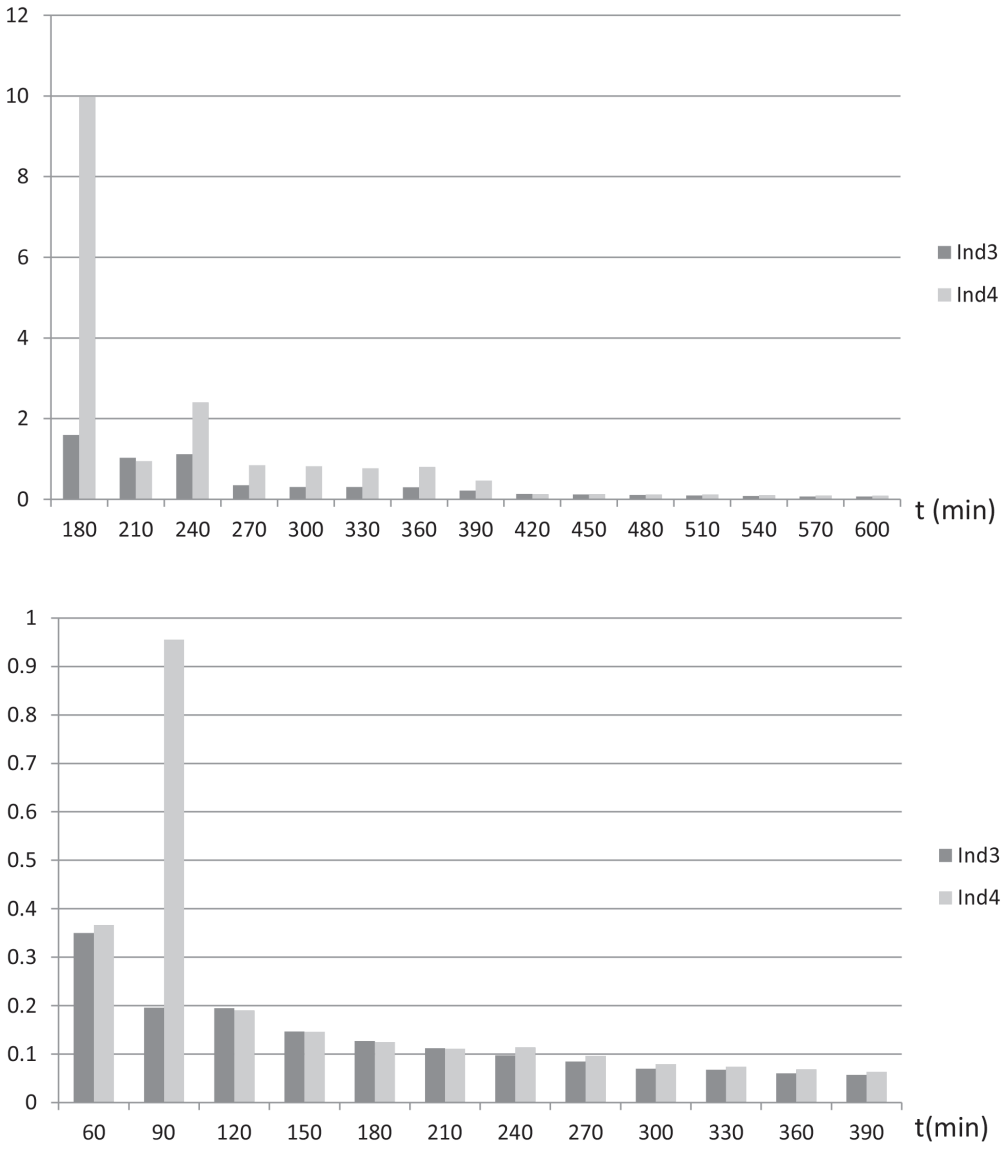

Fig. 6. Time evolution of i_3 and i_4 for scenarios 6 and 12.

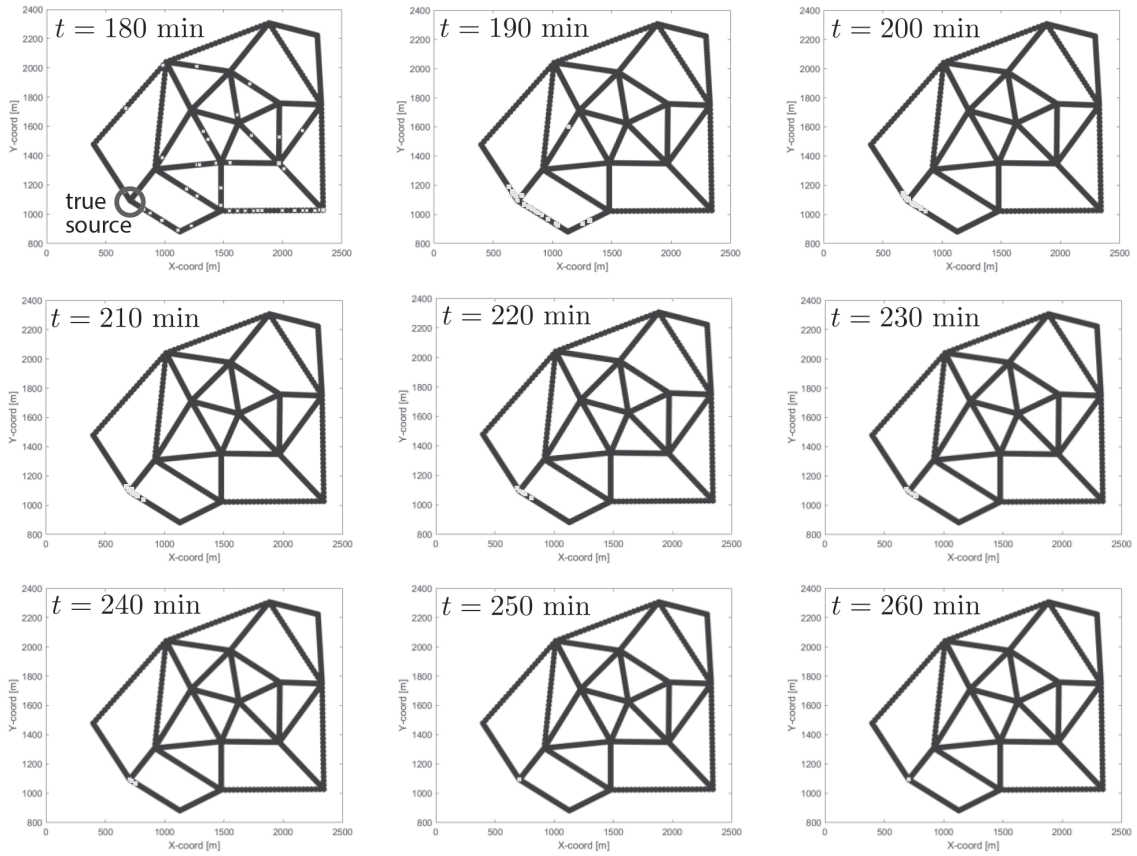

Fig. 7. Time evolution of the ensemble of source locations. Source positions shown by light squres.

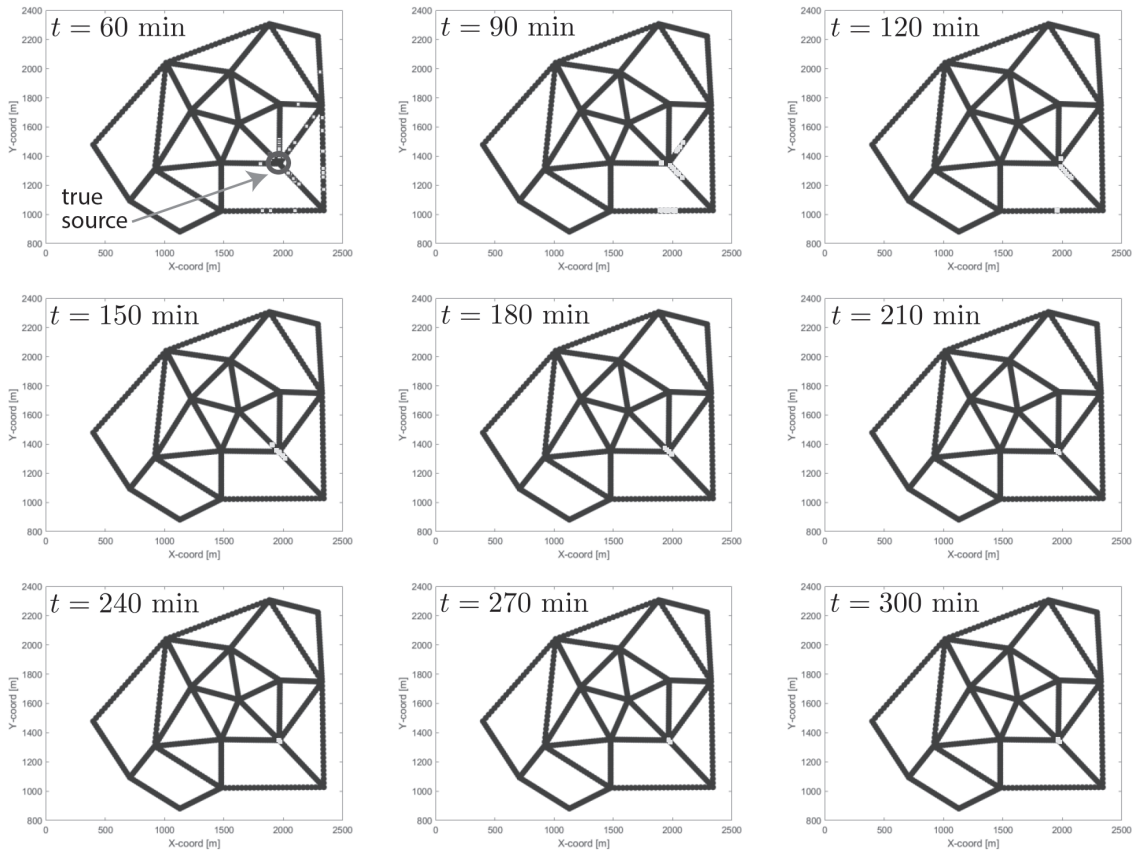

Fig. 8. Time evolution of the ensemble of source locations. Source positions shown by light squares.